2016 International Congress on Computation Algorithms in Engineering (ICCAE 2016)
ISBN: 978-1-60595-386-1

Analysis and Design of Low-Speed Direct-Driven Permanent-Magnet Submersible Motor

Shan Bai & Zhixiang Chang
School of Electrical Engineering, Shenyang University of Technology, Shenyang, Liaoning, China

ABSTRACT: This paper briefly introduces the structure of the low-speed permanent-magnet submersible motor and analyzes the relationship between the inner diameter of the stator and the copper loss of the motor after determination of the outer diameter of the stator and the length of the motor, in order to obtain the size of the inner diameter of the stator at the minimum copper loss. This paper also analyzes the relationship between the length of the magnetization direction of the permanent magnet and the size of the phase current, designs a set of 16-pole and 18-slot permanent-magnet submersible motor by the use of the above relationship and calculates the air-gap magnetic field, no-load counter electromotive force, electromagnetic torque and other properties by the use of the finite element method in order to verify the reasonableness of the motor design.

Keywords: permanent-magnet submersible motor; low-speed direct-driven; fractional slot concentrated winding electromagnetic performance

1 INTRODUCTION

Currently, China mainly adopts the way of mechanical petroleum recovery to exploit petroleum. Compared with other petroleum recovery equipment, the electric submersible screw pump for the petroleum recovery has the following advantages such as a wide applicable range of the well fluid, no roofbolt abrasion, convenient management and energy efficiency, which is especially suitable for the oil recovery in the heavy oil wells, sand wells, gas wells, horizontal wells and directional wells [1]. When the submersible screw pump operates at a low speed, the pump efficiency is high. For this purpose, the underground reduction gear is generally used, but the reducer is limited by the space, with more serious abrasion and shorter lifetime. Therefore, a new type of low-speed motor is developed to minimize the revolving speed of the submersible motor. The removal of the reduction gear can reduce the complexity of the petroleum recovery equipment and extend the inspection cycle of the oil well pump. Rare-earth permanent-magnet motor is suitable for the low-speed submersible motor. When the diameter of the motor is smaller, it is difficult to manufacture a multi-pole induction asynchronous motor. When the diameter of the motor is smaller, and the revolving speed is lower, the efficiency of the permanent-magnet motor is significantly higher than that of the asynchronous motor [2].

The power density and efficiency of the permanent-magnet synchronous motor with the fractional slot concentrated winding (FSCW) is higher and the length of the end is shorter, and the copper factor is higher, especially in the use of blocking stator, the copper factor can be higher. Moreover, a lower cogging torque has flux-weakening control ability and fault-tolerant ability. The above advantages make the permanent-magnet synchronous motor with the fractional slot concentrated winding achieve a considerable development in recent years [3-5]. In view of a smaller diameter of the submersible motor, it is impossible to open more slots at the stator side. Otherwise, it is difficult for the submersible motor with an elongated structure to complete threading, and it will also reduce the copper factor, and the torque density of the motor is limited. In the case of determination of the number of motor poles, the number of slots which is close to the number of poles is selected, the motor winding factor is higher and the torque density of the motor is greater. In addition, the combination with similar number of slots and poles will make them have a larger least common multiple, which will effectively reduce the cogging torque. The greatest common divisor of the number of poles and slots should be an

even number. Otherwise, the motor will produce an unbalanced radial magnetic pull. The selection of the number of slots and poles of the submersible motor shall comprehensively consider the above factors.

This paper analyzes the relationship between the inner diameter of the submersible motor stator and the copper loss of the windings, and also analyzes the impact of the length of the magnetization direction of the permanent magnet on the phase current of the motor. Appropriate motor parameters can be selected to reduce the copper loss of the motor and improve the motor efficiency. This paper also designs a set of 16-pole and 18-slot surface-mounted permanent-magnet submersible motor and calculates by the use of the finite element method in order to verify the reasonableness of the design.

2 BRIEF INTRODUCTION OF THE STRUCTURE OF SUBMERSIBLE MOTOR

The submersible motor operates in the oil well casing, and its outer diameter is limited by the inner diameter of the casing. The outer diameter of the common submersible motor is between 95mm and 188mm. If its length has fewer restrictions, the length of the motor may range from a few meters to decade meters based on the difference in the motor power. The submersible motor is an elongated structure. In order to avoid stator scrapping rotor and ensure the operational stability of the motor, the stator and rotor of the submersible motor is divided into a lot of segments. The length of stator and rotor in each segment is about 400mm. The magnetic isolated segment is between the stators in each segment, and the corresponding rotor side is alignment bearing. This design effectively reduces the risk of stator scrapping rotor. And the diagram below is a schematic diagram of two segments of the submersible motor:

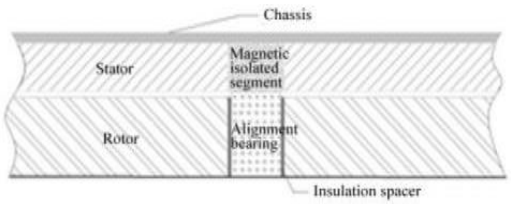

Figure 1. Schematic diagram of two segments of submersible motor.

3 MOTOR DESIGN

The submersible motor designed in this paper is 116 series of submersible motor, with an outer diameter of the motor of 116mm. It combines 16 poles with 18 slots. The quantity of slots per pole per phase of the motor (q) is 3/8, and its winding distribution coefficient (K_d) is 0.960, which is the same with that of the motor with three slots, the short-pitch factor is 0.985, and the winding coefficient (K_{dp}) is 0.945. The number of slots is similar to the number of poles, so the winding coefficient and power density are higher. It is different from 8-pole and 9-slot unit motor. The number of unit motor is not 1, so the motor is free of unbalanced radial magnetic pull. The diagram of star-connection for electric potential slot winding of the unit motor and the motor winding connection diagram are respectively shown in Figure 2 and Figure 3:

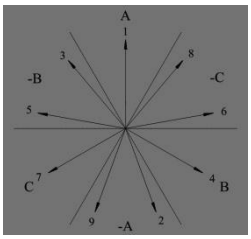

Figure 2. Diagram of star-connection for electric potential slot winding.

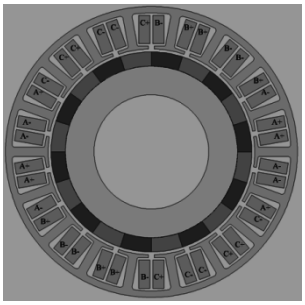

Figure 3. Motor winding connection diagram.

3.1 *Selection of inner diameter of stator*

After determination of the outer diameter and length of the motor, the selection of the inner diameter of the stator will directly affect the performance of the motor. Therefore, this paper first analyzes the relationship between the inner diameter of the stator and the copper loss of the motor in case of determination of the output power of the motor. The motor topological structure diagram is shown in Figure 4:

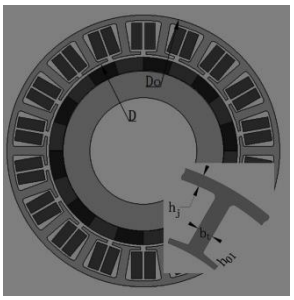

Figure 4. Motor topological structure diagram.

The main size of the motor is determined by the electromagnetic loads A and B_δ. After determination of the magnetic circuit structure of the rotor, the change of the air-gap flux density is small, the change of the magnetic load is small, and the inner diameter of the stator affects the value of the motor load (A) and winding wire diameter, thus affecting the copper loss of the motor. The relation between the main parameters of the motor is as follows [7]:

$$\frac{D^2 l_{ef} n}{P'} = \frac{6.1}{\alpha_p K_{Nm} K_{dp} A B_\delta} \tag{1}$$

Where, P' is the calculated power of the motor; n is the motor speed; l_{ef} is the effective length of the motor; a_p is the calculated pole-arc coefficient; K_{Nm} is the waveform factor of the air-gap magnetic field; B_δ is the air-gap flux density.

The following relation:

$$A = \frac{2mNI}{\pi D} \quad N = \frac{QN_c}{2ma} \quad I = a \cdot I_c \tag{2}$$

Substitute into the Formula (1):

$$N_c I_c = \frac{6.1\pi P'}{QDl_{ef} n\alpha_p K_{Nm} K_{dp} A B_\delta} \tag{3}$$

That is the size of total current of the conductors in each slot, of which Q is the quantity of slots of the stator, N is the number of series turns per phase, N_c is the number of conductors in each slot, I is the size of phase current size, and I_c is the size of current in the conductor.

Assuming that the flux density of the tooth part and the flux density of the yoke part are respectively B_t and B_j, the width of the tooth part and the height of the yoke part are respectively:

$$\begin{cases} b_t = \dfrac{\pi D B_\delta}{Q k_{Fe} B_t} \\ h_j = \dfrac{\pi D \alpha_p B_\delta}{4 p k_{Fe} B_j} \end{cases} \tag{4}$$

Where, k_{Fe} is the lamination factor of the silicon steel sheet.

By the use of the stator structure with a parallel tooth breadth as shown in Figure 4, the area of the stator slot is the ratio of the area and the quantity of slots (Q) after the annular area between the inner and outer diameter of the stator subtracting the area of the tooth part and the area of the yoke part after calculation by the following formula:

$$A_s = \left[\begin{array}{l} \pi\left(\dfrac{D_o - 2h_j}{2}\right)^2 - \pi\left(\dfrac{D + 2h_{01}}{2}\right)^2 \\ -Q \times b_i \times \left(\dfrac{D_o - D}{2} - h_j - h_{01}\right) \end{array} \right] \Big/ Q \tag{5}$$

Total copper loss of the motor can be expressed as follows:

$$P_{cu} = Q \cdot \left(N_c I_c\right)^2 \times \rho \times \frac{l}{A_s S_f} \tag{6}$$

Where, S_f is the copper factor, which is the ratio of the net area of the winding copper wire and copper area; l is the length of each conductor in the magnetic isolated segment and behind the ends of the submersible motor.

According to the Formula (6), the relationship between the copper loss of the motor and the inner diameter of the stator can be calculated by the use of Matlab, as shown in Figure 5:

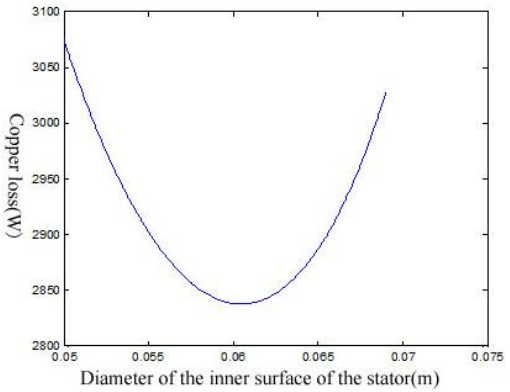

Figure 5. Relationship between the copper loss and the inner diameter of the stator.

According to the analytical result, when the inner diameter of the stator is small, the air-gap area transferred by the powered magnetic energy is small, the air-gap flux density remains constant, and there is a need of higher electrical load to achieve the same amount of electromagnetic power transfer, thus leading to the increase of total current of the stator in each slot and the copper loss of the stator. However, when the inner diameter of the stator is too large, the air-gap area used for the completion of the electromagnetic power transfer increases, and the number of total current in each slot reduces. In case of a constant copper factor, the sectional area of the winding will also reduce, and the resistance of the winding will increase, thus leading to the increase of the copper loss of the stator. According to the analytical result, reasonable selection of the inner diameter of the stator is vital for the decrease of the copper loss of the stator.

3.2 *Determination of quantity of conductors in each slot*

The submersible motor is powered by submersible cables. Generally, the cable length of the appropriate submersible motor is from 500m to 3,500m, which is limited by the underground space and economy. In addition, the sectional area of the submersible cable core shall not be too large. When the space of casing pipe is small or the pump hanging is deep, the voltage of the submersible motor, especially in the case of high-temperature wells, shall be improved as much as possible in order to ensure the operational reliability and efficiency of the submersible motor [8]. Therefore, increasing the number of series turns per phase and improve the operating voltage of the motor when we design is beneficial to reducing cable loss and increasing the economy of the petroleum recovery system.

In the case of ignoring the stator resistance, the electromagnetic torque of the non-salient pole permanent-magnet motor is [9]:

$$T_{em} = \frac{mpE_0U}{\omega X_s}\sin\theta \tag{7}$$

According to the Formula (7), in the case of determination of the torque angle (θ), the electromagnetic torque is mainly affected by the no-load counter electromotive force (E_0) and synchronous reactance (X_s). $X_s = \omega \cdot N^2 \cdot \Lambda$, $E_0 = 4.44 \cdot f \cdot N \cdot \Phi_{10}$, where: Λ is the magnetic permeance of the magnetic circuit, and Φ_{10} is the air-gap fundamental flux. With the increase of the number of winding turns, E_0 / X_s will reduce, and the amplitude of the electromagnetic torque will decrease, which is not conducive to the improvement of the starting torque of the motor, because it is a factor of limiting the increase of the number of winding turns. In addition, in view of the elongated structure of the submersible motor, it is very difficult for coil inserting, so the threading method is used for coil inserting. When there are a large number of turns designed, it is very difficult or even impossible to complete coil inserting. This is another important factor of limiting the increase of the number of turns.

According to the above analysis, the determination of the number of winding turns of the motor should comprehensively consider the capability of the motor output torque and power factor, and also try to increase the number of winding turns and improve the operating voltage of the motor, thus reducing the submersible cable loss.

3.3 *Determination of the length of magnetization direction of the permanent magnet*

The outer diameter of the rotor of the submersible permanent-magnet motor is small. In order to achieve low-speed direct-driven performance of the motor, the rotor is designed as 18 poles. When 18 poles are implemented in a smaller rotor, the use of the built-in rotor structure of the permanent-magnet may result in difficulty in rotor processing, reduction in the mechanical strength, and a large magnetic leakage coefficient [10], so this paper adopts the surface-mounted rotor structure. For the surface-mounted rotor structure, the length of the magnetization direction of the permanent magnet has a greater impact on the performance of motor. The operating speed of the submersible direct-driven motor is low, and the iron loss of the motor is small, so the impact of the permanent-magnet on the performance of the motor is mainly reflected in the impact on the power factor of the motor. A higher power factor may reduce the size of phase current, thus reducing the copper loss. Now, this paper analyzes the impact of the length of the magnetization direction of the permanent magnet on the phase current of the motor. In the case of the rated output power, the finite element method is used to calculate the relationship between the length of the magnetization direction of the permanent magnet and the phase current, as shown in Figure 6:

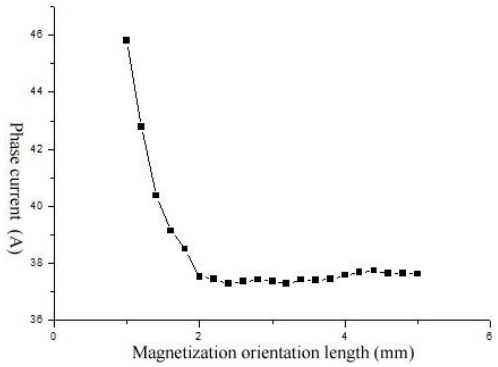

Figure 6. Relationship between the length of the magnetization direction of the permanent magnet and the phase current.

As can be seen from the calculation results of Figure 6, in the case of the rated output power, the length of the magnetization direction of the permanent magnet has a greater impact on the phase current of the motor. However, when the length of the magnetization direction of the permanent magnet reaches a certain value, the length of the magnetization direction of the permanent magnet will have a small impact on the phase current of the motor due to the influence of the magnetic saturation. Therefore, in design, there is a need to reasonably select the length of the magnetization direction of the permanent magnet. Inappropriate selection may lead to a low power factor and a large phase current, thus resulting in a large copper loss. In addition, in the selection of the length of the magnetization direction, there is also a need to check its ability to resist demagnetization and the work environment of

Table 1. Parameters of submersible permanent-magnet synchronous motor prototype.

Parameters	Value
Diameter of external surface of the stator yoke D_0 (mm)	102.4
Diameter of internal surface of the stator D (mm)	62
Height of stator yoke h_j (mm)	2.7
Width of tooth b_t (mm)	4.5
Air-gap length δ (mm)	0.75
Quantity of stator slot Q	18
Pole pairs of permanent-magnet p	8
Winding pitch (total tooth winding) y_1	1
Winding layer number	2
Parallel branch number a	1
Number of turns per coil N	6
Pole-arc coefficient of permanent-magnet α_p	1
Axial length of iron core of single motor L_e (mm)	400
Length of magnetic isolated segment L_g (mm)	45
Pitch number	15
Total length of motor L (m)	6.73
Model of permanent-magnet	SmCo28
Model of silicon steel sheet	DW310_35
Rated speed n (r/min)	375
Nominal voltage U_N (V)	560
Rated current amplitude I (A)	50
Power P (kw)	30

the motor. Under a higher work temperature, there is a need to increase the length of the magnetization direction of the permanent magnet, in order to ensure the air-gas flux density and the ability to resist demagnetization of the motor.

4 ELECTROMAGNETIC PERFORMANCE CALCULATION AND FINITE ELEMENT VERIFICATION

According to the above analysis, this paper designs a set of low-speed direct-driven submersible permanent-magnet motor. The parameters of the prototype are shown in Table 1.

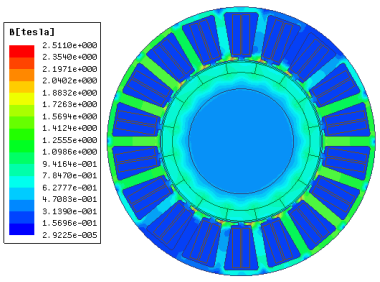

Figure 7. Distribution diagram of flux density at nominal load.

This paper calculates the prototype by the use of the finite element analysis software Maxwell in order to obtain the distribution diagram of the flux density as shown in Figure 7 and the distribution diagram of the air-gap magnetic flux density as shown in Figure 8 in case of the rated load of the prototype. The oscillogram of no-load counter electromotive force is shown in Figure 9, and the oscillogram of the electromagnetic torque is shown in Figure 11.

Figure 7 is the distribution diagram of the flux density of the motor under the rated condition calculated by Maxwell, of which the flux density of the motor tooth is 1.5T, and the flux density of the yoke is 1.4T.

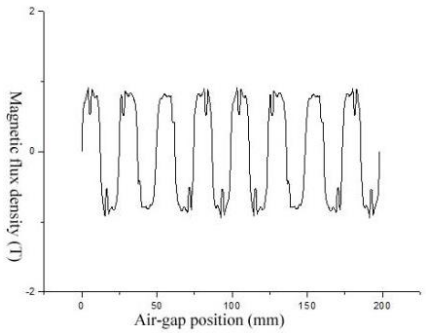

Figure 8. Distribution diagram of air-gap magnetic flux density.

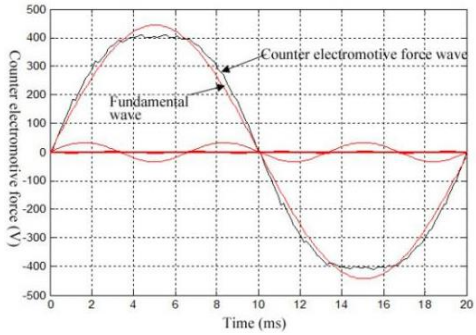

Figure 9. Oscillogram of no-load counter electromotive force.

As shown in the oscillogram of no-load counter electromotive force in Figure 9, its sine is better, and the result of its harmonic analysis is shown in Figure 10. As can be seen from Figure 10, the content of the third harmonic is higher, which is a main factor for causing waveform distortion of the counter electromotive force. And the content of other subharmonic is low.

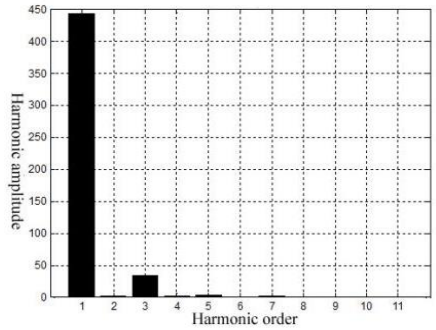

Figure 10. Harmonic analysis chart of no-load counter electromotive force.

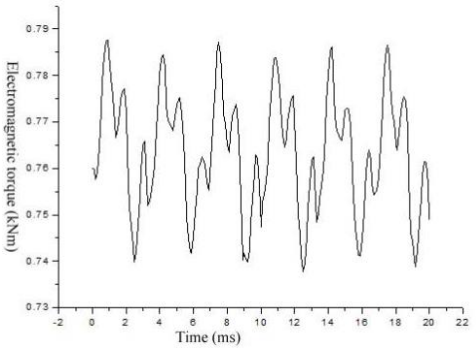

Figure 11. Electromagnetic torque diagram at a rated load.

Figure 11 is the steady-state torque of the motor calculated by the use of the finite element method. The torque ripple is defined as the difference between the maximum and minimum value of the torque and the ratio of the average torque. The simulation result shows that the torque ripple is 6.32%. This is because the magnetomotive force waveform of the phase winding is a rectangular wave after the use of the concentrated winding. Compared with the trapezoidal wave of the distributed winding, its harmonic content is higher, and the torque ripple of the concentrated winding is greater than that of the distributed winding.

5 CONCLUSION

This paper analyzes the impact of the inner diameter of the submersible motor stator and the length of the magnetization direction of the permanent magnet on the phase current of the stator, thus guiding the rational design of the low-speed direct-driven permanent-magnet submersible motor. This paper also calculates the submersible motor designed by the use of the finite element analysis software Maxwell, thus verifying the rationality of the design.

REFERENCES

[1] Wen J B. & Pan Y B. 2011. Research of six-pole permanent-magnet submersible motor design. *Proc Int Forum Strateg Technol, IFOST*, pp: 545-548.

[2] Thomas R B, Robert H M. & Trevor K. 2014. Induction versus permanent-magnet motors for electric submersible pump field and laboratory comparisons. *IEEE Transactions on Industry Application*, 50(1): 174-181.

[3] Ayman M EL Refaie. 2010. Fractional slot concentrated windings synchronous permanent-magnet machines opportunities and challenges. *IEEE Transactions on Industry Electronics*, 57(1): 107-121.

[4] Pia Salminen. 2004. *Fractional Slot Permanent-magnet Synchronous Motors for Low Speed Applications*. Acta University.

[5] Jiabin W, Xibo Yuan & Kais A. 2013. Design optimization of a surface-mounted permanent-magnet motor with concentrated windings for electric vehicle applications. *IEEE Transactions on Vehicular Technology*, 62(3): 1053-1064.

[6] K. Wang, Z.Q Zhu, Grzegorz O, M. Koch & Sunny Z. 2014. Electromagnetic performance of an 18-slot/10 -pole fractional-slot surface-mounted permanent-magnet machine. *IEEE Transactions on Industry Applications*, 50(6): 3685-3696.

[7] Chen Shikun. 2000. *Motor Design*. Second Edition. Beijing: Mechanical Industry Press, pp: 9-16.

[8] IEEE Std. 1984. 1018-1985. IEEE Recommended Practice for specifying Electric Submersible Pump cable/Ethylene Propylene Rubber Insulation. *Inst of Electrical and Electronics Engineers*.

[9] Jacek F. Gieras. 2010. *Permanent-magnet Motor Technology*. Third Edition. CRC Press.

[10] Tang Renyuan, et al. 1997. *Modern Permanent-magnet Motor Theory and Design*. Beijing: Mechanical Industry Press, 12: 162-170.